International Journal of Design & Nature and Ecodynamics
Vol. 21, No. 10, October, 2026, pp. 2847-2859
Journal homepage: http://iieta.org/journals/ijdne

Quarterly Spatiotemporal Assessment of Ecological Quality in a Tropical Nickel-Mining Landscape Using SCEQI: Pomalaa, Southeast Sulawesi, Indonesia, 2021–2025

La Gandri[1*], Lies Indriyani[1], Umar Ode Hasani[2], Vivi Fitriani[3], La Ode Muhammad Erif[1], Lucky Febriyanti[1], La Ode Anugrah[1], La Ode Siwi[1]

[1] Department of Environmental Science, Faculty of Forestry and Environmental Science, Halu Oleo University, Kendari 93232, Indonesia
[2] Department of Forestry, Faculty of Forestry and Environmental Science, Halu Oleo University, Kendari 93232, Indonesia
[3] Soil Science Study Program, Faculty of Agriculture, University of Jember, Jember 68121, Indonesia

Corresponding Author Email: lagandri@uho.ac.id

Copyright: ©2026 The authors. This article is published by IIETA and is licensed under the CC BY 4.0 license (http://creativecommons.org/licenses/by/4.0/).

https://doi.org/10.18280/ijdne.211002

Received: 27 July 2026
Revised: 6 October 2026
Accepted: 15 October 2026
Available online: 31 October 2026

Keywords:
ecological quality, Landsat, NDBSI, NDVI, nickel mining, Spatiotemporal Comprehensive Eco-Environmental Quality Index, Seasonal Mann–Kendall

ABSTRACT

Nickel mining is expanding rapidly in Indonesia, yet its effects on surface ecological quality are rarely tracked at seasonal resolution. This study assessed the Pomalaa nickel-mining landscape in Southeast Sulawesi using a quarterly Spatiotemporal Comprehensive Eco-Environmental Quality Index (SCEQI), built from Landsat 8/9 greenness, wetness, dryness, and heat indicators for 20 quarters (2021–2025). Ecological quality was lowest in mining-associated cells (annual SCEQI about 0.40–0.45), rose sharply within the 0–5 km belt, and levelled off at about 0.78–0.82 beyond 5 km, instead of increasing steadily with distance. Only the mining-associated cells showed a significant decline over time (Sen slope = −0.015 per year), driven by reduced vegetation greenness and expanding bare and dry surfaces. These findings support a two-tier monitoring design that treats mining cells and the adjacent 0–5 km belt as distinct management units with explicit remote-sensing warning indicators.

1. INTRODUCTION

Nickel is a strategic mineral for stainless steel, batteries, and clean-energy technologies. Demand for battery minerals continues to grow, and Indonesia has become both the centre of global nickel-production growth and the world's largest producer [1, 2], so changes in its nickel sector carry increasing economic and ecological consequences. However, expanding mineral supply for low-carbon technologies can intensify pressure on vegetation, soils, hydrology, and ecosystems in extraction areas. Across 7,721 villages in Sulawesi, deforestation in villages exposed to nickel mining was almost twice that of comparison villages, with mixed outcomes for well-being [3], and Southeast Sulawesi is among the provinces with high deforestation and loss of habitat for endemic biodiversity [4].

Pomalaa District, Kolaka Regency, is one of the most important nickel-mining and processing centres in Southeast Sulawesi. Between 2014 and 2023, forest and vegetation in the Pomalaa mining area decreased from 17,207.9 ha to 16,110.1 ha, while mine excavation increased from 1,792.3 ha to 2,005.4 ha and built-up/open land from 3,509.3 ha to 4,370.7 ha [5]. Monitoring is therefore needed that captures not only land-cover change but also repeated changes in surface ecological condition.

RSEI family and typical use. The Remote Sensing Ecological Index (RSEI) integrates greenness, wetness, dryness, and heat, generally represented by the Normalized Difference Vegetation Index (NDVI), wetness index (WET), Normalized Difference Built-up and Soil Index (NDBSI), and land surface temperature (LST), through principal component analysis (PCA) to reduce weighting subjectivity, and has been widely applied to urban, conservation, and mining areas [6, 7]. In nearby Kendari, Southeast Sulawesi, Landsat-derived NDVI was strongly negatively correlated with LST and positively with surface moisture [8]. Most applications compare one image or one composite per year and read the index as a relative measure of surface ecological condition.

Multi-temporal problems and why SCEQI matters. Conventional RSEI has limitations in multitemporal analysis: image-by-image normalisation changes the comparison basis between periods, a single image per year is affected by phenology and acquisition conditions, and the arbitrary sign of the PCA eigenvector may reverse the index interpretation [9]. Inconsistent eigenvector direction has been shown to bias ecological assessment [10], and the Continuous RSEI (CRSEI) was developed specifically to reduce multitemporal bias [11]. To improve spatiotemporal comparability, Li and Wang [9] proposed the Comprehensive Eco-Environment Quality Index Model with Spatiotemporal Characteristics (SCEQI), which combines full-sequence dimensionless normalisation, automatic PCA with control of component orientation, and multi-temporal averaging, making it suitable for large areas, long series, and dense intervals.

Mining landscapes and distance-buffer pitfalls. Ecological quality in open-pit mines can undergo distinct

phases of decline and recovery [12], and the differences observed around coal mines are greatest near the mining sites and attenuate with distance [13]. However, such thresholds are site-specific and cannot be directly transferred to tropical nickel-mining landscapes. Buffer analyses also tend to read values that rise with distance as a radius of influence, although the same pattern can arise from a sharp mining/non-mining contrast at the mine edge, and zone means from coarse cells blend mine and vegetation pixels. Three gaps exist: (1) annual or few-year intervals rarely separate seasonal variation from trend; (2) composite-index changes are often reported without their component indicators; and (3) few studies test whether a distance pattern is a continuous gradient or a local transition.

In response to these gaps, this study adapts SCEQI to the tropical nickel-mining landscape of Pomalaa through four analytical extensions: (1) SCEQI is computed for 20 quarterly periods during 2021–2025 using full-sequence normalisation, and trends are tested with the Seasonal Mann–Kendall test and Seasonal Sen slope so that seasonality is separated from temporal tendency (gap 1); (2) changes in the composite index are reported together with each component indicator (gap 2); (3) ecological conditions are compared across six non-overlapping distance zones and along a cell-level distance profile, to distinguish a local transition from a continuous gradient (gap 3); and (4) the robustness of the index is tested against the choice of normalisation range, PCA weighting, cloud masking, and spatial scale. The objectives are to (i) identify the spatiotemporal dynamics of NDVI, WET, NDBSI, LST, and SCEQI during 2021–2025; (ii) evaluate differences in ecological quality between the mining area and surrounding zones; (iii) quantify SCEQI change between consecutive years; and (iv) determine whether ecological change forms a continuous gradient with distance or a local ecological transition around the mining area.

2. MATERIALS AND METHOD

2.1 Study area and spatiotemporal design

The study covers the mining landscape and surrounding areas of Pomalaa District, Kolaka Regency, Southeast Sulawesi Province, Indonesia during 2021–2025. Each year is divided into four fixed quarters, Q1 (January–March), Q2 (April–June), Q3 (July–September), and Q4 (October–December), yielding 20 temporal units with identical seasonal positions across years.

Six non-overlapping zones were analysed (Figure 1): (1) mining-associated grid cells, (2) 0–5 km, (3) 5–10 km, (4) 10–20 km, (5) 20–30 km, and (6) 30–100 km, with distances measured from the outer boundary of the mining-associated cells. The 30–100 km zone represents regional ecological context and does not imply that mining influence extends causally to 100 km; distance-based buffers around mining areas are a common way to relate mining pressure to surrounding ecological conditions [14]. Because the final SCEQI resolution is 990 m, the mining area in the SCEQI analysis refers to grid cells associated with mining features rather than the precise footprint of mine openings; their derivation is described in Section 2.1.1.

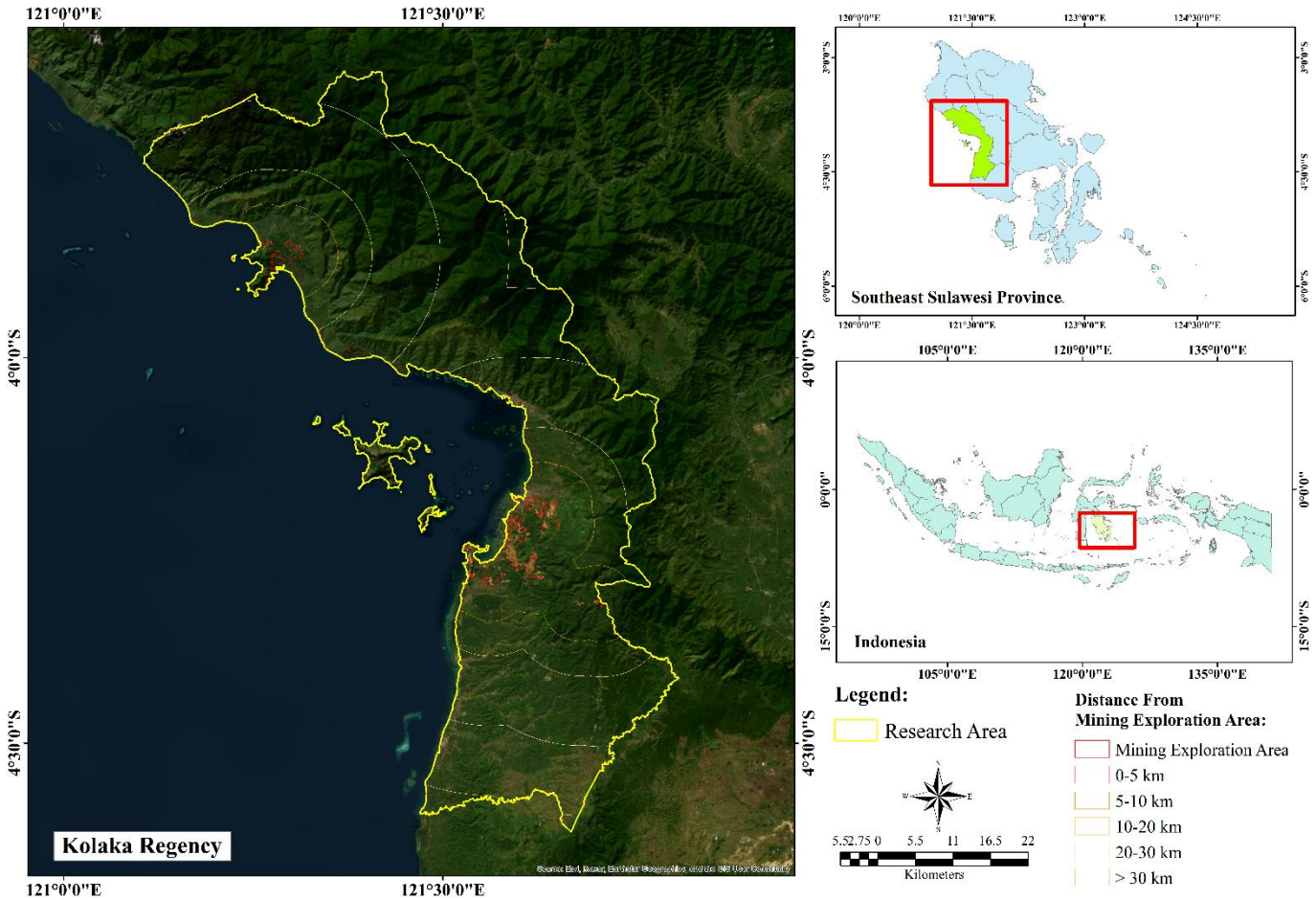

Figure 1. Study area and spatial analysis zones in the Pomalaa nickel-mining landscape, Southeast Sulawesi, Indonesia

Annual results are reported for all five years, 2021–2025, and year-to-year changes (2021–2022, 2022–2023, 2023–2024, and 2024–2025) are treated as neutral comparison periods. Because records that date mining stages (permits, production, or mapped excavation) were not available for the whole study window, the periods are not labelled as development phases. This is a descriptive temporal framework, not a difference-in-differences design or causal evidence of mining impact.

Definition of mining-associated grid cells. The mining-associated mask was produced in four steps (Supplementary Figure S1). (i) Source: mining features (open pits, stockpiles, haul roads, and processing areas) were digitised manually from the 2021–2025 Landsat 8/9 composites and high-resolution Google Earth imagery, and all features mapped in any year of the study period were merged into a single polygon layer. (ii) Cell assignment: a 990 m cell was classed as mining-associated when at least 50% of its area intersected a mining polygon. (iii) Temporal rule: the mask was held fixed for 2021–2025, so that every period compares the same 31 cells (about 30.4 km²) and SCEQI changes are not caused by changes in the mask itself. (iv) Buffers: the distance zones were generated from the outer boundary of the dissolved mask and made mutually exclusive. An example of the mask over the 30 m and 990 m grids is given in Figure S2.

2.2 Landsat data and pre-processing

The primary data were Landsat 8 and Landsat 9 OLI/TIRS Collection 2 images for 2021–2025. Pre-processing was performed in Google Earth Engine, which provides cloud computing for large-scale analysis of remote sensing archives [15]; further spatial analysis, raster aggregation, and zonal statistics were performed in ArcGIS Desktop 10.8 (Spatial Analyst) with Python 2.7 automation. Rasters were projected to WGS 84 / UTM Zone 51S (EPSG:32751) at a base resolution of 30 m.

Images were grouped by year and quarter. A quality-assurance mask removed fill pixels, dilated cloud, cirrus, cloud, cloud shadow, snow, and radiometrically saturated pixels. Where the strict-mask quarterly composite contained residual spatial gaps, a relaxed mask was applied only to pixels for which no valid strict-mask observation was available. The relaxed mask continued to exclude fill, cloud, cloud shadow, and radiometrically saturated pixels, but allowed observations flagged as dilated cloud or cirrus. Strict-mask observations always had priority, and fallback observations were drawn only from the same quarter; observations from other quarters or years were never used for gap filling. Valid observations within each quarter were summarized using a median composite to reduce sensitivity to individual acquisition dates while preserving the seasonal signal. Across the 20 quarterly composites, strict-mask coverage averaged 88.44%, ranging from 62.24% to 99.73%. The contribution of relaxed-mask pixels was generally small, averaging 0.95% in mining-associated cells and 4.67% in the 30–100 km zone. Only one quarter–zone observation exceeded a fallback contribution of 20% (30–100 km in 2023-Q1; 24.94%). Valid coverage and zone-specific fallback contributions are reported in Supplementary Table S1, and the trend analysis was repeated after excluding quarter–zone observations with fallback shares greater than 20%.

2.3 Ecological indicators

The indicator framework follows the RSEI/SCEQI structure, with NDVI and WET as positive ecological indicators and NDBSI and LST as indicators of ecological pressure [6, 9]. The operational equations below are identical to those of the processing pipeline that produced the study rasters, to ensure reproducibility.

2.3.1 Normalized Difference Vegetation Index

NDVI represents greenness:

$$NDVI = \frac{\rho_{NIR} - \rho_{Red}}{\rho_{NIR} + \rho_{Red}} \tag{1}$$

where, ρ_{NIR} and ρ_{Red} are near-infrared and red reflectance. Higher NDVI indicates a stronger vegetation signal.

2.3.2 Wetness index

WET describes the relative moisture response of vegetation, soil, and surface, and was computed consistently throughout 2021–2025 as:

$$\begin{aligned} WET = {} & 0.1511\rho_{Blue} + 0.2141\rho_{Green} + \\ & 0.0926\rho_{Red} + 0.0065\rho_{NIR} - 0.7529\rho_{SWIR1} \\ & - 0.5388\rho_{SWIR2} \end{aligned} \tag{2}$$

Higher (less negative) WET indicates relatively wetter surfaces. The coefficients are treated as the operational transformation of this study and were kept fixed for all periods.

2.3.3 Normalized Difference Built-up and Soil Index

NDBSI describes the combined signal of built-up, bare, and dry surfaces and is derived from the Index-based Built-up Index (IBI) and the Soil Index (SI). With band reflectances denoted by band names:

$$A = \frac{2SWIR1}{SWIR1 + NIR}, \qquad B = \frac{NIR}{NIR + Red} + \frac{Green}{Green + SWIR1} \tag{3}$$

$$IBI = \frac{A - B}{A + B} \tag{4}$$

$$SI = \frac{(SWIR1 + Red) - (NIR + Blue)}{(SWIR1 + Red) + (NIR + Blue)} \tag{5}$$

$$NDBSI = \frac{IBI + SI}{2} \tag{6}$$

Higher NDBSI indicates a stronger dry/bare/built-surface signal; the indicator is therefore treated as a negative ecological component.

2.3.4 Land surface temperature

LST was derived from Landsat Band 10 brightness temperature with NDVI-based emissivity correction. The vegetation fraction of mixed pixels is:

$$P_v = \left(\frac{NDVI - 0.20}{0.50 - 0.20}\right)^2, \quad 0.20 \le NDVI \le 0.50 \tag{7}$$

Surface emissivity was assigned piecewise:

$$\varepsilon = \begin{cases} 0.991, & NDVI < 0 \\ 0.970, & 0 \le NDVI < 0.20 \\ 0.986 + 0.004P_v, & 0.20 \le NDVI \le 0.50 \\ 0.990, & NDVI > 0.50 \end{cases} \quad (8)$$

and LST was calculated as:

$$LST = \frac{T_B}{1 + (\lambda T_B / c_2)\ln\varepsilon} - 273.15 \quad (9)$$

where, T_B is brightness temperature (K), $\lambda = 10.895 \times 10^{-6}$ m, and $c_2 = 1.438 \times 10^{-2}$ m K; results are expressed in ℃. This brightness-temperature–emissivity correction is the one used in the study pipeline and is not equivalent to the USGS Level-2 Surface Temperature product.

It was preferred because, to evaluate the consistency of the emissivity-corrected LST used in this study, LST derived from Eq. (9) was compared with Landsat 8/9 Collection 2 Level-2 Surface Temperature Band 10 (ST_B10). Monthly Level-2 observations were aggregated to the corresponding quarterly periods using a pixel-wise median and spatially aligned with the study-derived LST grid. Validation was restricted to spatially coincident pixels valid in both products. Values below 5 ℃ in either dataset were excluded as anomalous retrievals prior to sampling.

To avoid spatial overrepresentation by the larger outer zones, validation samples were selected using stratified random sampling by mining-distance zone and quarter. A maximum of 500 paired pixels was randomly selected from each of the six zones for each of the 20 quarterly periods using a fixed random seed, yielding 60,000 paired observations. Agreement was evaluated using Pearson's correlation coefficient (r), mean bias, and root mean square error (RMSE), where bias was defined as LST from Eq. (9) minus Level-2 ST_B10. The overall comparison showed a strong positive spatial correspondence (n = 60,000; r = 0.833), although the emissivity-corrected LST exhibited a systematic negative offset relative to ST_B10 (mean bias = −8.48 °C; RMSE = 9.35 ℃). Additional stratified comparisons by mining-distance zone and seasonal group are reported in Table S2.

2.4 Resolution harmonisation and scale sensitivity

SCEQI was constructed on a 990 m analysis grid. The 30 m NDVI, WET, NDBSI, and LST rasters were aggregated as the mean of the valid pixels within each 33 × 33 pixel block. The 990 m grid was kept as the main spatial support so that all analyses used identical geometry, and the native 30 m rasters were analysed as a scale-sensitivity test. Correlations of quarterly zonal means between 30 m and 990 m were 0.992 (NDVI), 0.978 (WET), 0.993 (NDBSI), and 0.970 (LST); aggregation therefore reduced local detail without altering the main between-zone and temporal patterns. Because mixed pixels are most frequent next to the mine, two further checks were made. First, the 0–5 km zone was split into 0–1, 1–3, and 3–5 km rings evaluated on the native 30 m grid. Second, SCEQI was rebuilt at two other aggregation scales, 450 m (15 × 15 pixels) and 1,980 m (66 × 66 pixels), to test whether the near-field pattern depends on the 990 m support (Table S3).

2.5 Full-sequence normalisation

To keep a single comparison basis across periods, all values of each indicator during 2021–2025 were used to define its global minimum and maximum. For indicator *j*:

$$\tilde{X}_{ijt} = \frac{X_{ijt} - X^{FS}_{j,\min}}{X^{FS}_{j,\max} - X^{FS}_{j,\min}} \quad (10)$$

where, X_{ijt} is the value of indicator *j* at pixel *i* and time *t*, and the superscript *FS* denotes the 2021–2025 full sequence. The ranges used were −0.3622 to 0.8174 (NDVI), −0.3481 to 0.0301 (WET), 0.1313 to 0.5878 (NDBSI), and 5.2002 to 34.8356 ℃ (LST). This adapts the full-sequence dimensionless method of Li and Wang [9], which preserves comparability between pixels and periods. Because global extremes can be inflated by residual artefacts, a sensitivity version used the 2nd and 98th percentiles of each indicator as the range and clipped values outside it; mining-area annual SCEQI and its trend were then recomputed (results in Section 3.9).

2.6 Principal component analysis and PC1 orientation

For each quarter, the four normalised indicators form the mean-centred matrix X_t, and PCA was computed from its covariance matrix and eigen-decomposition:

$$\mathrm{C}_t = \frac{1}{n-1}\mathrm{X}_t^T\mathrm{X}_t, \quad \mathrm{C}_t\mathrm{v}_{k,t} = \gamma_{k,t}\mathrm{v}_{k,t} \quad (11)$$

PCA reduces data dimensionality by maximising the variance captured by the principal components [16]. Because the eigenvector sign is not unique, PC1 orientation was controlled by NDVI: if the NDVI coefficient on PC1 was negative, the whole PC1 eigenvector was multiplied by −1:

$$\mathrm{v}'_{1,t} = \begin{cases} \mathrm{v}_{1,t}, & v_{NDVI,t} > 0 \\ -\mathrm{v}_{1,t}, & v_{NDVI,t} < 0 \end{cases} \quad (12)$$

$$PC1^{or}_{i,t} = \sum_{j=1}^{4} v'_{1,j,t}\tilde{X}_{ijt} \quad (13)$$

This direction control follows the SCEQI principle [9] and agrees with the finding that inconsistent eigenvector direction can bias PCA-based ecological assessment [10]. As an internal quality check (Table 1), quarters in which PC1 explained ≥60% of the variance and all four indicators loaded in the expected direction were rated “strong”. Quarters with ≥50% variance and expected directions were rated “moderate”, and all others were flagged for review. These are study-specific diagnostic rules, not universal PCA thresholds. Because separate PCAs per quarter allow the loadings to drift, the PC1 loadings of all 20 quarters are reported (Table S4), and two robustness versions were computed: (a) a pooled PCA fitted once to all 20 quarters, whose fixed loadings were applied to every quarter; and (b) trends recomputed after excluding the flagged quarters and, alternatively, after forcing a positive WET loading in those quarters (Table S5).

2.7 Quarterly Spatiotemporal Comprehensive Eco-Environmental Quality Index

All oriented PC1 values from the 20 quarters were renormalised using the full-sequence PC1 minimum and maximum:

$$SCEQI_{i,t} = \frac{PC1_{i,t}^{or} - PC1_{\min}^{FS}}{PC1_{\max}^{FS} - PC1_{\min}^{FS}} \quad (14)$$

so that $0 \le SCEQI \le 1$, with values near 1 representing relatively higher ecological quality and values near 0 relatively more degraded conditions.

Table 1. Internal labels used in quality control and sensitivity analyses

Label in Workflow	Plain-language Meaning	Location
Strong period (PASS_STRONG)	PC1 explains ≥60% of variance and all four indicators load in the expected direction	Section 2.6; Table 2
Moderate period (PASS_MODERATE)	PC1 explains 50% to <60% of variance and all directions are as expected	Section 2.6; Table 2
Flagged period (REVIEW)	At least one indicator loads against its ecological meaning (here always WET)	Sections 2.6 and 3.2; Table S5
Main annual product (MAIN n ≥ 2)	Annual mean requires at least two valid quarters at the pixel	Sections 2.8 and 3.5
Strict annual product (STRICT n ≥ 3)	Annual mean requires at least three valid quarters; sensitivity check	Sections 3.1 and 3.5
All observations (ALL_VALID)	Trend test uses every valid quarter regardless of coverage	Sections 2.10 and 3.9; Table 3
Coverage-filtered	Trend test uses only quarter–zone observations with ≥50% valid area	Sections 2.10 and 3.9

Note: WET = wetness index.

2.8 Annual Spatiotemporal Comprehensive Eco-Environmental Quality Index and year-to-year change

Annual SCEQI was computed as the temporal mean of valid quarters at each pixel:

$$SCEQI_{i,y} = \frac{1}{n_{i,y}} \sum_{q=1}^{4} S\,CEQI_{i,y,q}, \quad n_{i,y} \ge 2 \quad (15)$$

The main annual product requires at least two valid quarters at a pixel (Eq. (15)); a stricter version requiring at least three valid quarters was produced as a sensitivity check (Table 1). No spatial interpolation or artificial gap filling was performed. Change between years was computed as $\Delta SCEQI = SCEQI_{y2} - SCEQI_{y1}$ for 2021–2022, 2022–2023, 2023–2024, and 2024–2025, with negative values indicating decline.

2.9 Ecological-quality classes

Continuous SCEQI was classified with a constant interval of 0.20 so that changes in class area reflect changes in index values rather than shifting thresholds: very low (0.00–0.20), low (0.20–0.40), moderate (0.40–0.60), high (0.60–0.80), and very high (0.80–1.00). Five-level classification is common in RSEI time-series studies for distinguishing ecological conditions and class changes [17]. The 0.20 interval follows the equal-interval convention of RSEI studies [17]; because SCEQI is a relative PCA-based score, class names describe relative position within this landscape rather than absolute ecological states. As a sensitivity check, classes were also defined by quintiles of the pooled 2021–2025 SCEQI distribution (Table S6).

2.10 Zonal statistics and coverage

For every combination of indicator, period, and zone, the mean, standard deviation, minimum, maximum, number of valid cells, valid area, and coverage (valid area as a percentage of zone grid area) were computed. Coverage was rated good (≥80%), moderate (50% to <80%), or low (<50%). The main trend analysis used all valid observations and was repeated with only observations of ≥50% coverage as a sensitivity analysis.

2.11 Seasonal Mann–Kendall test and Seasonal Sen slope

Because the series consists of four recurring quarters, trends were analysed with the Seasonal Mann–Kendall test. For each quarter q:

$$S_q = \sum_{i=1}^{n_q-1} \sum_{j=i+1}^{n_q} \operatorname{sgn}\left(X_{jq} - X_{iq}\right) \quad (16)$$

$$\operatorname{sgn}(x) = \begin{cases} 1, & x > 0 \\ 0, & x = 0 \\ -1, & x < 0 \end{cases}, \qquad S = \sum_{q=1}^{4} S_q \quad (17)$$

The seasonal Kendall approach suits seasonal data, tolerates missing values, and does not assume normality [18]. Trend magnitude was estimated with the Seasonal Sen slope, comparing only the same quarter across years:

$$\beta_{Sen} = \operatorname{median}\left(\frac{X_{j,q} - X_{i,q}}{t_j - t_i}\right), \quad j > i \quad (18)$$

Sen's slope is a robust, median-based estimator of pairwise slopes [19]. The null hypothesis of no monotonic trend was rejected at $p < 0.05$. The analysis was applied to SCEQI and all four indicators.

2.12 Distance-gradient analysis

Mean annual SCEQI in the six zones was paired with representative distances of 0, 2.5, 7.5, 15, 25, and 65 km, and monotonic association was tested with Spearman's rank correlation (r_s). The analysis was run for all six zones and for the five zones outside the mining area, to distinguish a sharp mining-versus-surroundings contrast from a genuinely continuous gradient in the surrounding zones. Because six zone means give little statistical power, the analysis was repeated at cell level: every 990 m cell outside the mask was assigned the Euclidean distance from its centroid to the nearest mask boundary, cells were grouped into 1 km bins to 10 km, 2.5 km bins to 30 km, and 10 km bins to 100 km, and bin means with 95% confidence intervals were plotted (Figure S3). Spearman's r_s between cell distance and SCEQI was computed separately for cells within 0–5 km and beyond 5 km; because neighbouring cells are spatially autocorrelated, these cell-level p-values are treated as indicative.

3. RESULTS

SCEQI ranges from 0 to 1; higher values mean greener, wetter, cooler, and less bare surfaces relative to the whole 2021–2025 landscape. Results move from the component indicators (Sections 3.3–3.4) to the composite index (3.5–3.7) and its spatial and temporal structure (3.8–3.9). The central pattern is summarised in Figure 2: SCEQI is low in the mining-associated cells, rises sharply within 0–5 km, and stays on a high plateau beyond 5 km instead of increasing steadily with distance.

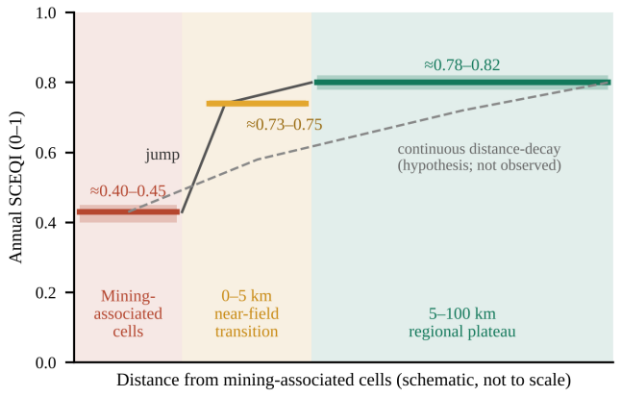

Figure 2. Conceptual summary of annual Spatiotemporal Comprehensive Eco-Environmental Quality Index (SCEQI) with distance: Mining-associated deficit, near-field transition, and regional plateau (ranges from 2022–2025 zone means)

3.1 Data quality control and cross-scale stability

Four indicators (NDVI, WET, NDBSI, and LST) were produced for each of the 20 quarterly composites, giving 4 × 20 = 80 native 30 m rasters; each was then aggregated to the 990 m grid by block mean (Section 2.4), giving 80 corresponding harmonised 990 m rasters. All 80 native 30 m and 80 harmonised 990 m rasters passed checks of cell size, grid dimension, extent, and coordinate system, and quarterly zonal means at the two resolutions were highly correlated (r = 0.970–0.993). Coverage was 77.59–100.00% for the main annual product and 46.55–100.00% for the stricter product. The largest sensitivity occurred in the 30–100 km zone in 2023 (0.8189 at 96.55% coverage versus 0.7323 at 53.45%), so annual values for the outermost zone are interpreted cautiously as regional context.

Across the 20 quarterly composites, the strict QA mask alone retained an average of 88.44% of analysis-grid cells. The relaxed fallback contribution was generally small, averaging 0.95% of final valid pixels in the mining-associated cells and 4.67% in the 30–100 km zone, where fallback use was highest (Table S1). Only one quarter–zone observation exceeded a fallback contribution of 20% (30–100 km in 2023-Q1;24.94%). Excluding observations exceeding this threshold did not change either the direction or statistical significance of the mining-area SCEQI trend; the fallback-filtered result was identical to the main analysis (τ = −0.550, Sen Slope= −0.01475 y^{-1}, p = 0.0101; Table S5).

3.2 Principal component analysis characteristics

PC1 explained 51.11–77.92% of the variance of the four indicators, with a mean of 65.17% (Table 2). Across the 20 quarterly periods, 14 were rated strong, two moderate, and four were flagged for review (2021-Q1, 2021-Q4, 2022-Q4, and 2024-Q2). In all four flagged periods, the directional mismatch involved only WET, whereas NDVI, NDBSI, and LST retained the expected ecological directions (Table S4). The mean oriented PC1 coefficients were +0.621 for NDVI, +0.143 for WET, −0.697 for NDBSI, and −0.278 for LST (Table 2). These coefficients indicate that the dominant structure of ecological variation was primarily a greenness–dryness/bare-surface contrast, with thermal stress contributing negatively and WET showing a smaller and more variable contribution. Across quarters, the coefficients ranged from +0.467 to +0.745 for NDVI and from −0.732 to −0.644 for NDBSI, whereas WET showed the greatest directional variability, ranging from −0.074 to +0.377 (Table S4).

As an additional temporal-comparability check, a pooled PCA fitted to all 20 quarters explained 60.14% of the total variance and produced fixed PC1 coefficients of +0.561 for NDVI, +0.223 for WET, −0.712 for NDBSI, and −0.357 for LST (Table S4). The resulting pooled-PCA SCEQI remained strongly correlated with the quarter-specific SCEQI series (r = 0.872) and retained a significant declining trend in the mining-associated area (Seasonal Kendall τ = −0.600, Sen slope = −0.01374 y^{-1}, p = 0.0048; Table S5). These results indicate that the main temporal pattern was not an artefact of quarter-to-quarter variation in PCA coefficients.

Table 2. Summary of Spatiotemporal Comprehensive Eco-Environmental Quality Index (SCEQI) principal component analysis (PCA), 2021–2025

Component	Mean / Range	Interpretation
PC1 explained variance	65.17% (51.11–77.92%)	Majority of the variance of four indicators
PC1 coefficient NDVI	+0.621	Positive ecological direction
PC1 coefficient WET	+0.143	Positive; more variable
PC1 coefficient NDBSI	−0.697	Negative; largest magnitude
PC1 coefficient LST	−0.278	Negative ecological direction
Quality rating	14 / 2 / 4	Strong/moderate/flagged (Table 1)

Note: NDVI = Normalized Difference Vegetation Index; WET = wetness index; LST = land surface temperature.

3.3 Contrasts in ecological components with distance

On the 990 m grid, the mining area differed consistently from the surrounding zones. Mean 2021–2025 NDVI was 0.390 in the mining area, 0.632 at 0–5 km, and 0.677–0.703 in zones ≥5 km, whereas mean NDBSI reached 0.417 in the mining area, compared with 0.279 at 0–5 km and 0.254–0.273 further away. Mean LST was 23.87 °C in the mining area, 22.08 °C at 0–5 km, and 21.12–21.58 °C in zones ≥5 km, while mean WET was −0.151 in the mining area compared with about −0.098 to −0.108 elsewhere. These contrasts recur in most quarters (Figure 3).

3.4 Trends in Spatiotemporal Comprehensive Eco-Environmental Quality Index component indicators

The Seasonal Mann–Kendall test showed that the most consistent indicator changes were concentrated in the mining area. NDVI declined strongly (τ = −0.80; Sen slope =

−0.01482 y^{-1}; p = 0.00015), whereas NDBSI increased significantly (τ = 0.70; +0.00688 y^{-1}; p = 0.00094), indicating persistent loss of greenness and an increasingly dry/bare surface. LST in the mining area had a positive slope of about +0.241 °C y^{-1} that was not significant (p = 0.391), and WET showed no significant trend. Temporal change in the mining area is thus marked by declining NDVI and increasing NDBSI rather than by monotonic thermal or moisture trends.

With coverage ≥50%, NDVI in the mining area still declined (−0.01514 y^{-1}; p = 0.00015), and NDBSI still increased (+0.00600 y^{-1}; p = 0.00268). An NDVI increase in the 20–30 km zone with all valid observations (+0.00327 y^{-1}; p = 0.01996) lost significance after coverage filtering (p = 0.0678) and is not treated as robust.

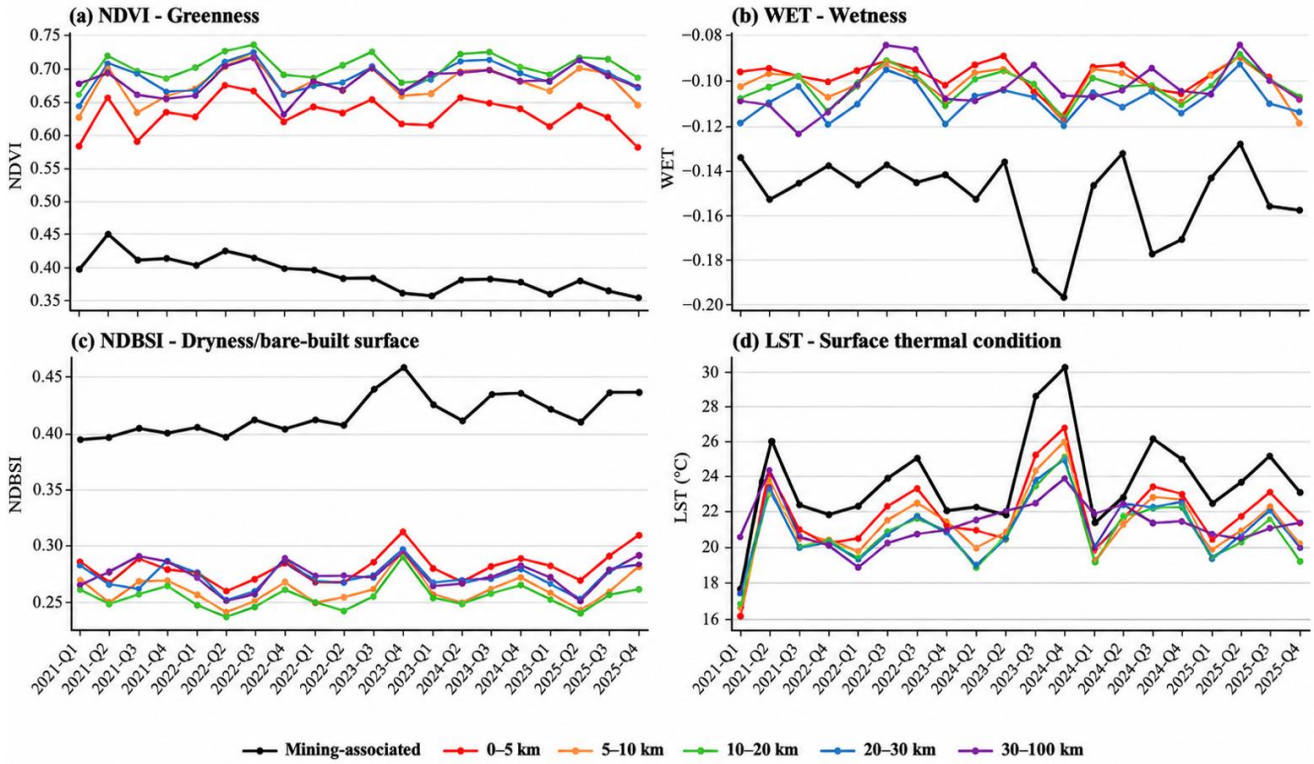

Figure 3. Quarterly dynamics of NDVI, WET, NDBSI, and LST in the six distance zones, 2021–2025
Note: NDVI = Normalized Difference Vegetation Index; WET = wetness index; NDBSI = Normalized Difference Built-up and Soil Index; LST = land surface temperature.

3.5 Annual Spatiotemporal Comprehensive Eco-Environmental Quality Index, 2021–2025

Integration of the four indicators revealed a pronounced difference in ecological quality between the mining-associated area and its surroundings (Figures 4 and 5). The reconstructed annual SCEQI for 2021 was 0.500 in the mining-associated area. The 2021 values are reconstructed annual estimates and are reported for reference only; the class-composition (Section 3.7) and distance-gradient (Section 3.8) analyses and Figure 2 are based on 2022–2025. Mining-area SCEQI subsequently decreased from 0.449 in 2022 to 0.404 in 2023, increased slightly to 0.414 in 2024, and remained low at 0.410 in 2025. The 0–5 km zone had a reconstructed annual SCEQI of 0.760 in 2021 and remained within a relatively narrow range of 0.731–0.748 during 2022–2025, while zones ≥5 km were mostly within 0.784–0.819. Thus, the spatial contrast between the mining-associated area and its surroundings was substantially larger than the interannual variability observed in most non-mining zones.

Comparison of the main annual product, calculated from at least two valid quarters, with the stricter product requiring at least three valid quarters showed that results for the mining-associated area and near-mine zones were relatively stable. The 30–100 km zone was the most sensitive to the number of valid quarters, with the largest difference occurring in 2023 (0.8189 for the main product versus 0.7323 for the stricter product; difference = 0.0866). Fluctuations in this outermost zone are therefore interpreted cautiously as regional variability rather than evidence of a linear radius of mining influence.

3.6 Spatiotemporal Comprehensive Eco-Environmental Quality Index change between consecutive years

SCEQI change was not fully monotonic. In 2021–2022, mining-area SCEQI decreased by −0.0506, representing the largest consecutive-year decline in the mining-associated area during the study period. In 2022–2023, the mining area declined further (ΔSCEQI = −0.0453), compared with only −0.0032 at 0–5 km; the 5–20 km zones increased slightly, while the 30–100 km zone increased by +0.0110. In 2023–2024, the mining area showed a partial recovery (+0.0100), whereas the 30–100 km zone declined by −0.0075. In 2024–2025, mining-area SCEQI decreased slightly again (−0.0044); the largest decline occurred in the 0–5 km zone (−0.0161), while the 5–20 km zones remained nearly stable. Overall, the sequence indicates repeated ecological deterioration in the mining-associated area interrupted by only a modest recovery in 2024.

3.7 Changes in ecological-quality class composition

A redistribution of ecological classes accompanied changes in continuous SCEQI values. In 2022, 45.16% of the mining-

associated cells were classified as very low + low, 35.48% as moderate, and 19.35% as high + very high. By 2025, the high + very high share had declined to only 6.45%, while the moderate share increased to 51.61% and the very low + low share remained high at 41.94% (Figure 6). The main compositional change within the mining-associated area was therefore not simply an expansion of the lowest classes, but a marked reduction in high-quality cells accompanied by a shift toward the moderate class.

In 2025, the high + very high share was 6.45% in the mining-associated area, compared with 81.35% at 0–5 km, 94.69% at 5–10 km, 97.27% at 10–20 km, 90.02% at 20–30 km, and 93.33% at 30–100 km. Under the pooled-quintile classification, however, the proportion of mining-associated cells in the two highest classes was 0% in both 2022 and 2025; all mining-associated cells fell within the two lowest quintiles of the pooled 2021–2025 landscape distribution (Table S6). Thus, the exact magnitude of the decline in the high + very high share is sensitive to the fixed 0.20 class thresholds, but the broader conclusion that the mining-associated area occupies the lower end of the regional ecological-quality distribution is robust to the alternative classification scheme.

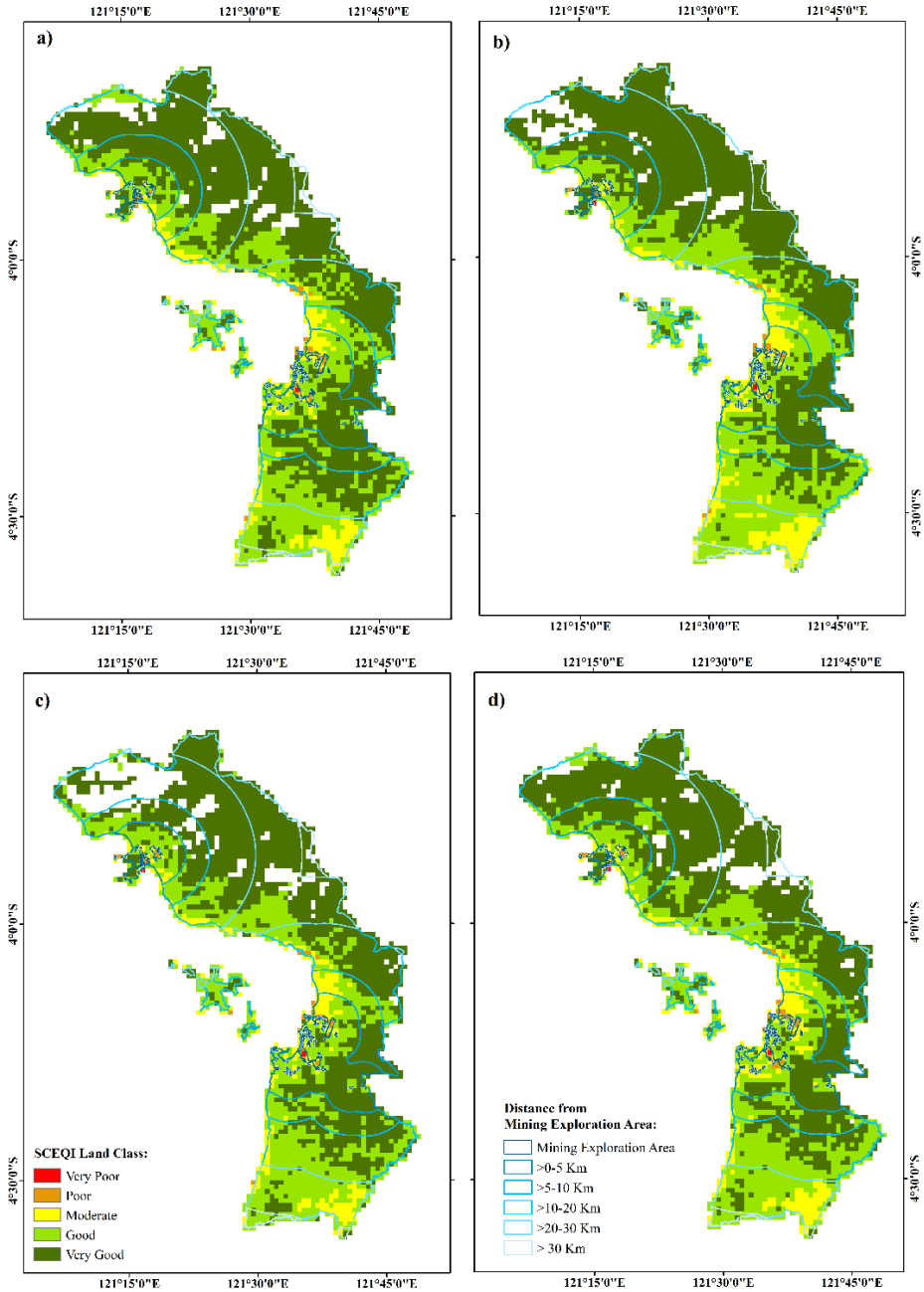

Figure 4. Spatial distribution of annual continuous Spatiotemporal Comprehensive Eco-Environmental Quality Index (SCEQI) across the Pomalaa mining landscape, 2021–2025

3.8 Spatial gradient with distance

When all six zones were analysed, SCEQI tended to increase with distance, with a significant relationship in 2023 and 2024 (r_s = 0.829, p = 0.042), but not in 2022 and 2025 (r_s = 0.543, p = 0.266). When the mining-associated area was excluded, the distance–SCEQI relationship was non-significant in every year; in 2023 and 2024, for example, r_s decreased to 0.700 (p = 0.188). These results indicate that the significant all-zone relationship was driven largely by the markedly lower SCEQI of the mining-associated area. Among the non-mining zones, differences were comparatively small

and did not follow a consistent monotonic gradient (Figure 5). The spatial pattern is therefore better characterized by a pronounced ecological contrast at the mining boundary, followed by a rapid near-field increase in SCEQI and relatively stable values at greater distances, rather than by a continuous distance-decay relationship extending to 100 km.

Finer-scale analyses supported this interpretation. Based on the cell-level SCEQI values summarized into distance bins, mean SCEQI increased rapidly within the first 5 km from the mining-mask boundary. The correlation between distance-bin position and mean SCEQI within this near-field interval was strong (r_s = 0.90), with mean SCEQI increasing from 0.69 in the 0–1 km bin to approximately 0.79 within the 3–5 km interval. Beyond 5 km, the relationship between distance-bin position and mean SCEQI was much weaker (r_s= 0.35), and values fluctuated within a relatively narrow range rather than increasing consistently with distance (Figure S3). On the native 30 m grid, mean SCEQI increased gradually from 0.632 in the 0–1 km ring to 0.659 at 1–3 km and 0.680 at 3–5 km. The strong contrast between mining-associated cells and surrounding areas, followed by substantially smaller differences among the outer zones, was also retained at 450 m and 1,980 m spatial supports (Table S3). This cross-scale consistency indicates that the observed near-mine contrast was not an artefact of the principal 990 m analysis grid.

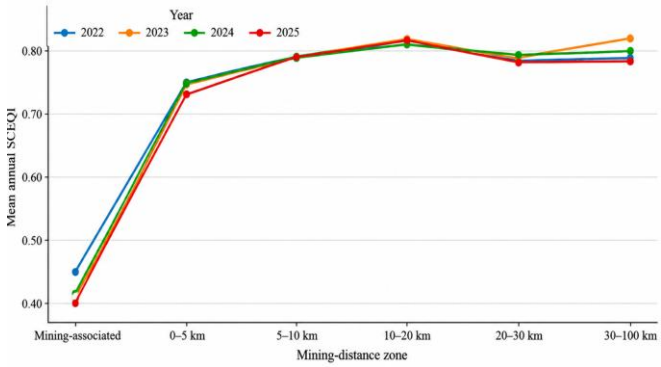

Figure 5. Spatial profile of mean annual Spatiotemporal Comprehensive Eco-Environmental Quality Index (SCEQI) across the six distance zones, 2021–2025

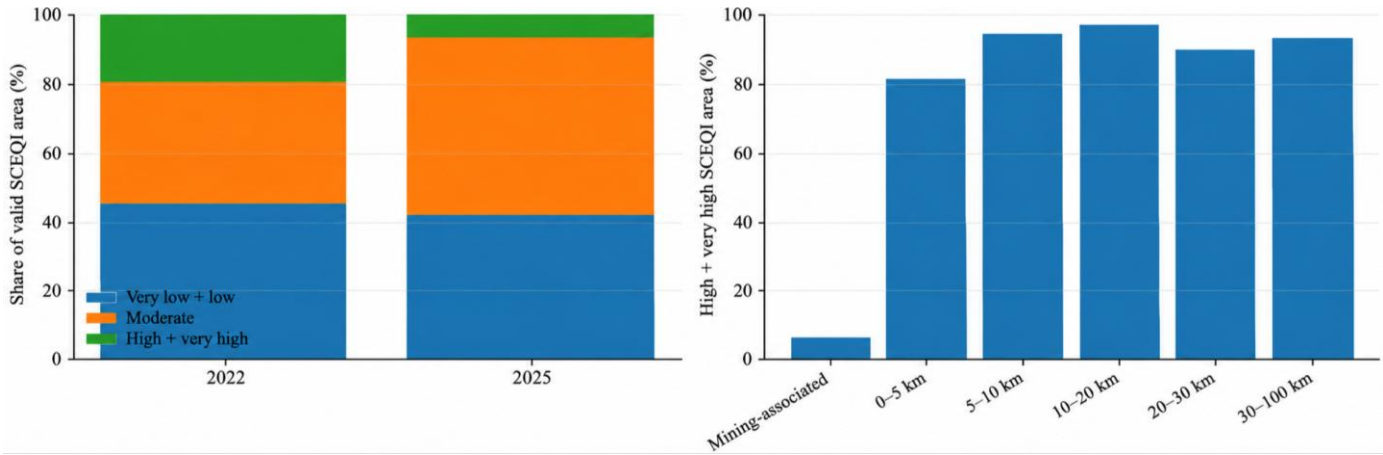

Figure 6. Spatiotemporal Comprehensive Eco-Environmental Quality Index (SCEQI) class composition: (a) mining area in 2022 and 2025; (b) high + very high share by zone in 2025

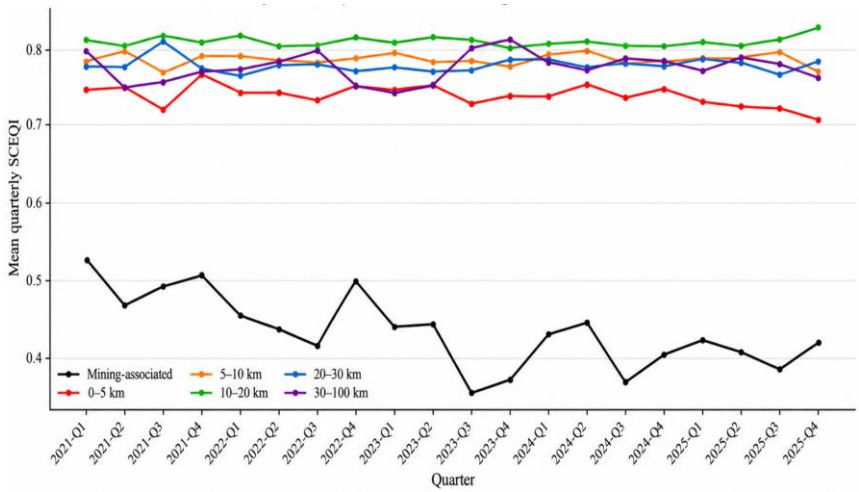

Figure 7. Quarterly Spatiotemporal Comprehensive Eco-Environmental Quality Index (SCEQI) dynamics in the six zones, 2021–2025

3.9 Spatiotemporal Comprehensive Eco-Environmental Quality Index trends, 2021–2025

Across the 20 quarterly observations (Figure 7), only the mining-associated area showed a significant SCEQI trend (τ = −0.55; Sen slope = −0.01475 y^{-1}; p = 0.0101; Table 3). The 0–5 km zone also showed a negative but non-significant trend (Sen slope = −0.00346 y^{-1}; p = 0.1779), whereas the 5–10 km

and 10–20 km zones showed little net change, and the 20–30 km and 30–100 km zones showed small, non-significant positive slopes. After restricting the analysis to observations with ≥50% spatial coverage, the mining-area decline remained significant (Sen slope = −0.01185 y^{-1}; $p = 0.0265$), indicating that the observed negative trend was not driven by variation in spatial coverage.

Table 3. Seasonal Mann–Kendall test and Sen slope of Spatiotemporal Comprehensive Eco-Environmental Quality Index (SCEQI), 2021–2025

Zone	τ	Sen Slope (y^{-1})	p	Trend
Mining-associated	−0.550	−0.01475	0.0101	Significant decrease
0–5 km	−0.300	−0.00346	0.1779	Decrease, n.s.
5–10 km	−0.050	−0.00022	0.9025	Stable
10–20 km	−0.050	−0.00064	0.9025	Stable
20–30 km	+0.150	+0.00122	0.5403	Slight increase, n.s.
30–100 km	+0.050	+0.00152	0.9025	Slight increase, n.s.

Note: n.s. = not significant at $\alpha = 0.05$; all valid observations ($n = 20$ quarters).

The mining-area decline was partly robust to alternative analytical choices (Table S5). Under 2nd–98th percentile normalization, the decline became slightly stronger (Sen slope = −0.01913 y^{-1}; $p = 0.0022$). Using pooled PCA with fixed coefficients also retained a significant negative trend (Sen slope = −0.01374 y^{-1}; $p = 0.0048$). When the four quarters flagged for anomalous WET direction were excluded, the slope remained negative (−0.01107 y^{-1}), but the trend was no longer statistically significant ($p = 0.1032$). Excluding quarter–zone observations with more than 20% fallback pixels produced a slope of −0.01475 y^{-1}; $p = 0.0101$, identical to the main analysis because no mining-area quarter exceeded the 20% fallback threshold. Overall, the direction and approximate magnitude of the decline were stable across sensitivity tests, although its statistical significance was sensitive to complete removal of the four WET-flagged quarters.

4. DISCUSSION

4.1 The ecological deficit of the mining area is multidimensional

The low SCEQI of the mining area reflects several indicators at once: lower NDVI and WET and higher NDBSI and LST, with robust temporal decline in NDVI and increase in NDBSI. This is consistent with surface clearing, where vegetation loss weakens the vegetation signal while bare soil, built surfaces, and haul roads strengthen NDBSI; loss of shading and evapotranspiration also explains the spatially higher LST, consistent with the negative NDVI–LST relationship reported for Kendari [8] and with mine-specific indices that combine vegetation, soil, and temperature signals to track mine disturbance [20]. Because the LST trend was not significant after seasonality was removed by comparing the same quarter across years [18, 19], the results indicate a persistent thermal contrast rather than monotonic warming. These findings agree with evidence that nickel mining amplifies forest loss in Sulawesi [3] and with local reports of expanding excavation and open land in Pomalaa [5].

4.2 Spatiotemporal Comprehensive Eco-Environmental Quality Index mainly represents a greenness–dryness contrast

The PC1 structure (Table 2) indicates that the dominant ecological gradient primarily separates greener conditions from dry/bare surfaces. The PC1 coefficients arise from the covariance structure of the indicators within each quarter rather than from predefined weights, thereby reducing subjectivity in indicator weighting [16], while the orientation of PC1 to a positive NDVI direction maintains a consistent ecological interpretation across periods [9, 10]. The four flagged quarters involved a directional mismatch only in WET, whereas NDVI, NDBSI, and LST retained their expected ecological directions, and PC1 continued to explain more than 50% of the total variance (Table S4).

These quarters were retained in the primary analysis because the dominant PC1 structure remained ecologically interpretable and their complete removal would reduce the seasonal time series from 20 to 16 observations. When the four flagged quarters were excluded, the mining-area Sen slope remained negative (−0.01107 y^{-1}), but the trend was no longer statistically significant ($p = 0.1032$). In contrast, retaining these observations while forcing the WET coefficient to the expected positive direction produced a negative trend and yielded an SCEQI series that was almost identical to the primary series ($r = 0.999$; Table S5). Thus, the direction of the mining-area decline is not dependent on the anomalous WET signs, although its statistical significance is sensitive to the complete removal of the four flagged quarters.

The pooled PCA provides an additional fixed-weight benchmark. It explained 60.14% of the variance and produced the same expected ecological directions for all four indicators (Table S4). The pooled-PCA SCEQI was strongly correlated with the quarter-specific index ($r = 0.872$) and retained a significant negative mining-area trend ($p = 0.0048$; Table S5). This agreement indicates that the main temporal pattern is unlikely to be an artefact of quarter-to-quarter variation in PCA coefficients.

4.3 Ecological change is non-monotonic between years

Mining-area SCEQI fell sharply in 2022–2023, rebounded slightly in 2023–2024, and declined again in 2024–2025, consistent with the non-linear trajectories reported for open-pit mines [12]. The 2023–2024 increase cannot be interpreted as successful reclamation without independent data on reclamation sites or mining activity; it may reflect regrowth, shifts in activity, moisture changes, or their combination. Linking these year-to-year changes to mining stages would require permit, production, or mapped excavation records, which is a priority for follow-up work.

4.4 The 0–5 km zone as a near-field ecological transition

The distance–SCEQI relationship disappears once the mining area is excluded: quality rises steeply to 0–5 km and the 5–100 km zones form a relatively high plateau, whereas a continuous decay of mining influence would produce a monotonic increase up to 30–100 km. As reported by Chai et al. [13], change is strongest near the mines, but distance thresholds depend on mine type, landscape, climate, and

topography and are not universal radii. The 0–5 km zone is therefore best described as a near-field transition zone and more distant zones as regional context, not as evidence of a causal radius of influence.

4.5 Class shifts reveal ecological-quality erosion

In the mining area, the high + very high share fell from 19.35% to 6.45% while the moderate share rose to 51.61%, so degradation proceeded mainly as an erosion of high quality towards the moderate class rather than direct conversion to very low quality. Such transitions can provide an early signal of decline before very low quality dominates, as graded classes have been used to track disturbance and recovery in RSEI time series [17], and moderate rather than very low classes have been found to dominate disturbed opencast-mining areas [21].

Table 4. Remote-sensing warning signals and triggered actions for the two management units

Management Unit and Warning Signal	Remote-sensing Condition	Triggered Field Check or Action
Mining cells: active clearing	SCEQI falls by >0.05 against the same quarter of the previous year, or NDVI declines in four consecutive same-quarter comparisons	Field verification of new clearing; compare with the approved mining and reclamation plan
Mining cells: bare-surface expansion	NDBSI rises by >0.02 with stable or rising LST	Inspect haul roads and stockpiles; dust suppression and erosion-control structures
0–5 km belt: class downgrade	A cell moves from the high/very high to the moderate class in two consecutive quarters	Ground check for encroachment, sediment deposition, or drainage change; report to the environmental agency
0–5 km belt: drying signal	WET declines while LST rises in the dry-season quarter (Q3)	Sample turbidity and sediment at downstream points; review runoff and settling ponds
Both units: data quality	Valid coverage <50% or fallback share >20% in a quarter	Treat the signal as provisional; confirm with Sentinel-2 or field photographs before action

Note: Thresholds are initial values proposed for calibration with field data. NDVI = Normalized Difference Vegetation Index; NDBSI = Normalized Difference Built-up and Soil Index; WET = wetness index; LST = land surface temperature.

4.6 Implications for environmental management

The results translate into a two-tier monitoring framework in which the mining-associated cells and the 0–5 km transition belt are treated as separate management units (Table 4). In the mining cells, the priority is to detect where clearing outpaces revegetation; in the 0–5 km belt, it is to catch spill-over before quality falls towards mining-cell levels. Each warning signal is a quarterly remote-sensing condition that triggers a defined field check, so the index works as a screening tool. Remote-sensing indices provide spatial early warning but do not replace field measurement of water, soil, heavy metals, and biodiversity [3]; heavy-metal accumulation has already been reported in the coastal waters and corals off Pomalaa [22].

4.7 Limitations

SCEQI describes surface condition (greenness, wetness, dryness, and heat) and does not directly measure heavy metals, water or air quality, biodiversity, or ecosystem function. The design is observational, so mining-area contrasts indicate strong association rather than proof of causation, as topography, rainfall, land use, and non-mining development may also contribute. The 990 m grid reduces local detail and does not represent the exact extent of mine openings, although the finer-ring and multi-scale checks (Table S3) address this in part. Five years is short for long-term inference; four PCAs showed an unexpected WET direction (tested in Table S5), and cloud contamination remains a constraint that full-sequence normalisation and multi-temporal averaging reduce but do not eliminate [9].

5. CONCLUSIONS

Quarterly SCEQI identified both spatial differences and temporal changes in ecological quality in the Pomalaa nickel-mining landscape during 2021–2025. The mining area consistently had the lowest ecological quality, and its mean SCEQI fell from 0.449 in 2022 to 0.410 in 2025, with a significant trend of $-0.01475\ y^{-1}$ ($p = 0.010$) accompanied by an NDVI decline of $0.01482\ y^{-1}$ and an NDBSI increase of $0.00688\ y^{-1}$ (both $p < 0.001$). LST and WET differed spatially but had no significant trend, so the most persistent change is reduced greenness and increasingly dry/bare surfaces.

Ecological quality rises steeply from the mining area to the surrounding zones but does not form a monotonic gradient across 5–100 km. The spatial structure is best interpreted as a strong mining-associated ecological deficit followed by a near-field transition, rather than as evidence of continuous mining influence up to 100 km. In the mining area, the combined share of high and very high classes decreased from 19.35% to 6.45%, accompanied by a corresponding increase in the moderate class, indicating ecological-quality erosion even in the absence of dominance by the lowest classes.

The combined SCEQI framework provides a practical basis for periodic monitoring of rapidly changing mining landscapes; treating mining cells and the 0–5 km belt as management units with explicit warning signals turns it into an operational screening tool. It should be complemented by field, pollution, biodiversity, and reclamation data and extended with longer series and mining-operation records to strengthen impact attribution.

DATA AVAILABILITY

Landsat 8 and Landsat 9 Collection 2 data are freely available from the USGS and in Google Earth Engine as LANDSAT/LC08/C02/T1_L2 and LANDSAT/LC09/C02/T1_L2 for surface reflectance; LANDSAT/LC08/C02/T1_TOA and LANDSAT/LC09/C02/T1_TOA for Band 10 brightness temperature. The strict mask used QA_PIXEL bits 0–5 (fill, dilated cloud, cirrus, cloud, cloud shadow, snow) and QA_RADSAT for saturation. The relaxed fallback mask was applied only to pixels with no valid strict-mask observation in

the same quarter; it continued to exclude fill, cloud, and cloud shadow (QA_PIXEL bits 0, 3, and 4) and radiometrically saturated pixels (QA_RADSAT), but accepted observations flagged as dilated cloud (bit 1) or cirrus (bit 2). Quarterly composites were per-pixel medians of valid observations within each calendar quarter. The mining-associated mask, zone polygons, quarterly 990 m indicator and SCEQI rasters, and zonal statistics tables are available in the Supplementary Material.

CODE AVAILABILITY

The Google Earth Engine script used for quality masking, quarterly compositing, and indicator calculation is provided as Supplementary Code S1. The Python 2.7 scripts used with ArcGIS Desktop 10.8 (arcpy, Spatial Analyst) for raster aggregation, PCA, SCEQI calculation, zonal statistics, and trend tests are provided as Supplementary Code S2. Both are published with the Supplementary Material of this study.

ACKNOWLEDGMENT

The authors would like to express their sincere gratitude to the Ministry of Higher Education, Science, and Technology of the Republic of Indonesia for funding this research through the Fundamental Research Program (FPR) under the BIMA research grant scheme, as per decree No. 226/C3/DT.05.00/PL-BARU/2026 and contract No. 44/DST/UN29.23/PG/2026. The authors also thank all parties who contributed to and supported the implementation of this research.

REFERENCES

[1] International Energy Agency. (2025). Global critical minerals outlook 2025. IEA, Paris. https://www.iea.org/reports/global-critical-minerals-outlook-2025.

[2] U.S. Geological Survey. (2026). Mineral commodity summaries 2026. U.S. Geological Survey, Reston, Virginia, USA. https://doi.org/10.3133/mcs2026

[3] Lo, M.G.Y., Morgans, C.L., Santika, T., et al. (2024). Nickel mining reduced forest cover in Indonesia but had mixed outcomes for well-being. One Earth, 7(11): 2019-2033. https://doi.org/10.1016/j.oneear.2024.10.010

[4] Supriatna, J., Shekelle, M., Fuad, H.A.H., et al. (2020). Deforestation on the Indonesian island of Sulawesi and the loss of primate habitat. Global Ecology and Conservation, 24: e01205. https://doi.org/10.1016/j.gecco.2020.e01205

[5] Sofyan, A.B., Fadlin, F., Arifin, D., Insanu, R.K., Sutaji, A.A.M. (2024). Mapping deforestation and land cover change in the nickel mining area of Pomalaa District using remote sensing technology [in Indonesian]. Journal of Geomatics Engineering, Technology, and Science, 2(2): 50-55. https://doi.org/10.51967/gets.v2i2.35

[6] Fang, G., Pablo II, R.D.A., Zhang, Y. (2023). Eco-environmental quality assessment using the remote sensing ecological index in Suzhou City, China. Sustainability, 15(17): 13158. https://doi.org/10.3390/su151713158

[7] Jiang, L.N., Zhang, J.N., Wang, S.J., Zhang, J.B., Li, X.L. (2025). Spatiotemporal dynamics of eco-environmental quality and driving factors in China's Three-North Shelter Forest Program using GEE and GIS. Sustainability, 17(17): 7698. https://doi.org/10.3390/su17177698

[8] Indriyani, L., Kete, S.C.R., Isabela, Fitriani, V., Gandri, L., De Ahmaliun, L. (2025). Impacts of vegetation dynamics on land surface temperature and moisture in Kendari City, Indonesia: A remote sensing study. International Journal of Design & Nature and Ecodynamics, 20(10): 2315-2323. https://doi.org/10.18280/ijdne.201010

[9] Li, N., Wang, J.Y. (2022). Comprehensive eco-environment quality index model with spatiotemporal characteristics. Sensors, 22(24): 9635. https://doi.org/10.3390/s22249635

[10] Guo, Y.Z., Zhan, M.J., Xu, H., et al. (2025). $MRSEI_{LA}$: A modified remote sensing ecological index using local adaptability for enhancing ecological environment quality assessment. Ecological Informatics, 90: 103238. https://doi.org/10.1016/j.ecoinf.2025.103238

[11] Jin, W., Li, H.Z., Wang, J.Z., et al. (2023). Continuous remote sensing ecological index (CRSEI): A novel approach for multitemporal monitoring of eco-environmental changes on a large scale. Ecological Indicators, 154: 110739. https://doi.org/10.1016/j.ecolind.2023.110739

[12] Wang, X.B., Nian, Y.Y., Wang, H.Y., et al. (2025). Monitoring of ecological environment changes in open-pit mines on the Loess Plateau from 1990 to 2023 based on RSEI. Ecological Indicators, 170: 113064. https://doi.org/10.1016/j.ecolind.2024.113064

[13] Chai, H.B., Zhao, Y.Q., Xu, H., et al. (2024). Analysis of ecological environment in the Shanxi section of the Yellow River Basin and coal mining area based on improved remote sensing ecological index. Sensors, 24(20): 6560. https://doi.org/10.3390/s24206560

[14] Li, J.Q., Tian, Y. (2024). Assessment of ecological quality and analysis of influencing factors in coal-bearing hilly areas of northern China: An exploration of human mining and natural topography. Land, 13(7): 1067. https://doi.org/10.3390/land13071067

[15] Gorelick, N., Hancher, M., Dixon, M., Ilyushchenko, S., Thau, D., Moore, R. (2017). Google Earth Engine: Planetary-scale geospatial analysis for everyone. Remote Sensing of Environment, 202: 18-27. https://doi.org/10.1016/j.rse.2017.06.031

[16] Jolliffe, I.T., Cadima, J. (2016). Principal component analysis: A review and recent developments. Philosophical Transactions of the Royal Society A: Mathematical, Physical and Engineering Sciences, 374(2065): 20150202. https://doi.org/10.1098/rsta.2015.0202

[17] Lin, L., Hao, Z., Post, C.J., Mikhailova, E.A. (2022). Monitoring ecological changes on a rapidly urbanizing island using a remote sensing-based ecological index produced time series. Remote Sensing, 14(22): 5773. https://doi.org/10.3390/rs14225773

[18] Hirsch, R.M., Slack, J.R., Smith, R.A. (1982). Techniques of trend analysis for monthly water quality data. Water Resources Research, 18(1): 107-121. https://doi.org/10.1029/WR018i001p00107

[19] Sen, P.K. (1968). Estimates of the regression coefficient

based on Kendall's tau. Journal of the American Statistical Association, 63(324): 1379-1389. https://doi.org/10.1080/01621459.1968.10480934
[20] Zhang, P.P., Chen, X.D., Ren, Y., Lu, S.Q., Song, D.W., Wang, Y.L. (2023). A novel mine-specific eco-environment index (MSEEI) for mine ecological environment monitoring using Landsat imagery. Remote Sensing, 15(4): 933. https://doi.org/10.3390/rs15040933
[21] Xiao, W., Guo, J.W., He, T.T., Lei, K.G., Deng, X.Y. (2023). Assessing the ecological impacts of opencast coal mining in Qinghai-Tibet Plateau: A case study in Muli coal field, China. Ecological Indicators, 153: 110454. https://doi.org/10.1016/j.ecolind.2023.110454
[22] Riska, R., Tasabaramo, I.A., Zamani, N.P., Lalang, Syadiah, E.A. (2022). Accumulation of heavy metals (Pb, Cd, Hg) in coral Acropora aspera at Pomalaa waters, Southeast Sulawesi [in Indonesian]. Jurnal Ilmu dan Teknologi Kelautan Tropis, 14(1): 69-80. https://doi.org/10.29244/jitkt.v14i1.37553

NOMENCLATURE

A, B	dimensionless ratio terms of IBI and SI
C_t	covariance matrix of normalised indicators
c_2	second radiation constant, 1.438×10^{-2} m K
LST	land surface temperature, ℃
n	number of valid pixels or observations
NDBSI	Normalized Difference Built-up and Soil Index
NDVI	Normalized Difference Vegetation Index
P_v	vegetation fraction
r_s	Spearman rank correlation coefficient
S	Mann–Kendall statistic
SCEQI	spatiotemporal comprehensive eco-environmental quality index
T_B	brightness temperature, K
t	time, y
v	eigenvector
WET	wetness index
X	indicator value

Greek symbols

β_{Sen}	Seasonal Sen slope, y^{-1}
γ	eigenvalue
ε	land surface emissivity
λ	effective wavelength of Band 10, m
ρ	surface reflectance
τ	Kendall's tau

Subscripts

FS	full sequence 2021–2025
i, j	pixel, indicator
q, t, y	quarter, period, year